Probing nuclear shapes close to the fission limit with the giant dipole resonance in ^{216}Rn

M. Kmiecik,[1] A. Maj,[1] B. Million,[2] M. Brekiesz,[1] W. Królas,[1] W. Męczyński,[1] J. Styczeń,[1] M. Ziębliński,[1] A. Bracco,[2] F. Camera,[2] G. Benzoni,[2] S. Leoni,[2] O. Wieland,[2] S. Brambilla,[2] B. Herskind,[3] M. Kicińska-Habior,[4] N. Dubray,[5] J. Dudek,[5] and N. Schunck[6]

[1]*The Niewodniczański Institute of Nuclear Physics, Polish Academy of Sciences, ul. Radzikowskiego 152, 31-342 Kraków, Poland*

[2]*Dipartimento di Fisica, Universitá di Milano and INFN Sez. Milano, Via Celoria 16, 20133 Milano, Italy*

[3]*The Niels Bohr Institute, Blegdamsvej 15-17, 2100 Copenhagen, Denmark*

[4]*Institute of Experimental Physics, Warsaw University, Warsaw, Poland*

[5]*Institut de Recherches Subatomiques and Louis Pasteur University, 23 rue du Loess, BP28 F-67037, Strasbourg Cedex 2, France*

[6]*Department of Physics, 30BC04, University of Surrey, Guildford GU2 1XH, United Kingdom*

(Received 25 February 2004; published 17 December 2004)

The gamma-ray decay of the giant dipole resonance (GDR) in the compound nucleus ^{216}Rn formed with the reaction ^{18}O+^{198}Pt at the bombarding energy of 96 MeV was investigated. High-energy gamma-ray spectra in coincidence with both prompt and delayed low-energy transitions were measured. The obtained GDR width at the average temperature $\langle T\rangle \approx 1$ MeV was found to be larger than that at $T=0$ MeV and to be approximately constant as a function of spin. The measured width value of 7 MeV is found to be consistent with the predictions based on calculations of the nuclear shape distribution using the newest approach for the treatment of the fission barrier within the liquid drop model. The present study is the first investigation of the giant dipole resonance width from the fusion-evaporation decay channel in this nuclear mass range.

DOI: 10.1103/PhysRevC.70.064317 PACS number(s): 21.60.Ev, 24.10.Lx, 24.30.Cz, 24.60.Dr

I. INTRODUCTION

The mechanism of nuclear fission induced by fast rotation and the nuclear shape evolution on the way to scission is an interesting and still open question. The giant dipole resonance (GDR) has proven to be sensitive to the average nuclear shapes at finite temperature and therefore it represents an adequate tool to study this problem [1–3]. Nuclear deformations corresponding to the saddle point configurations are often expected to be very large. The related experimental information is particularly interesting as it provides a sensitive test of both the macroscopic methods of calculating the total nuclear energy at high temperatures as well as the microscopic ones taking into account thermal excitations.

The term "fission limit" used throughout this paper applies by definition to the spin value, say I_f, for which the fission-barrier penetrability from the static equilibrium deformation equals 50%. Within a model, such a spin can be relatively easily determined in the calculations but much less so through measurement. In no place in this paper will the *precise value* of such an experimental parameter be needed. Calculation results and their comparison with experiment suggest that in the present context $I_f \sim 40\,\hbar$, within a few $\hbar$ inaccuracy.

In order to obtain information about the nuclear shape evolution along the fission path, it is possible to use at least two different approaches. One of them consists in studying the GDR in fissioning nuclei, by measuring the GDR decay during the fission process. From the high-energy γ-ray spectra in coincidence with the fission products, in principle one may expect to obtain the information about the shape of fissioning nuclei and thus about their shape evolution along the fission path. However, the existing data show that this is not at all an easy task because of the presence in the spectra of the γ rays from the fission products [4,5].

Another approach consists in measuring the GDR decay in the fusion-evaporation process by selecting very high spins around the critical spin value at which the fission process is beginning to dominate. Such measurements are also in general very difficult, because one has to select a very narrow spin window and at the same time to reject the fission contamination. This can be achieved by tagging either on the fusion-evaporation products or on the γ rays from specific residual nuclei. So far, investigations of this type have provided high-energy γ-ray spectra through gating on different residual nuclei (see, e.g., the case of ^{194}Hg [6]). However, they have not allowed for the spin selection in a narrow region close to the fission limit.

In this paper, we present the results of an experiment on the GDR γ decay associated with high spins around the fission limit. For this purpose, we choose the fusion-evaporation reaction ^{18}O+^{198}Pt at the bombarding energy of 96 MeV, populating with rather high cross-section residual nuclei characterized by the presence of long-lived high-spin isomeric states. The decaying ^{216}Rn compound nucleus, selected in the present study, strongly feeds the isomeric states of $I=30$ in ^{212}Rn and $I=63/2$ in ^{211}Rn. In addition, since only two feeding transitions to these isomeric states were found [7], one expects that the fission limit in ^{216}Rn is below or around 40 $\hbar$. Therefore, the selection of the GDR γ decay in coincidence with delayed γ-ray transitions is expected to probe mainly the compound nuclei which survive fission, yet with angular momenta close to the fission limit.

It should be noted that the isomer tagging technique used in the present work has been successfully employed in lighter-mass nuclei to select the particular areas of the phase space of the decay, leading to specific nuclear deformations [8].

In the following, we present the GDR data concerning the compound ^{216}Rn nucleus, and discuss the resulting inclusive

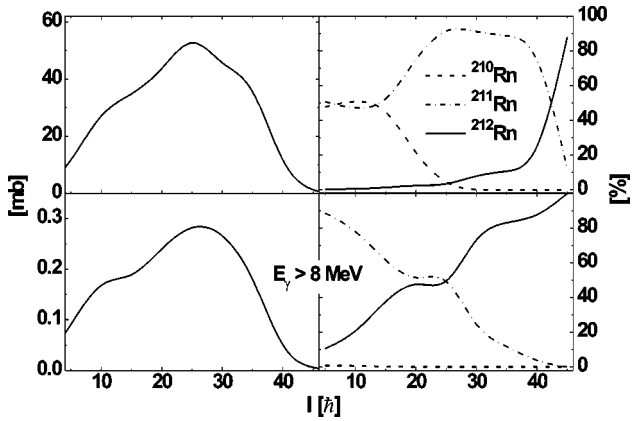

FIG. 1. Calculated cross sections for the population of evaporation residues in ^{212,211,210}Rn as functions of spin: with no condition on γ-ray energy (top) and with the gate on γ-ray energy in the GDR region (bottom).

and exclusive (isomer tagged) spectra. We find it attractive to perform the investigations in this heavy mass region, in particular for ^{216}Rn, for which the theory predicts a rather unexpected shape evolution as a function of angular momentum up to the fission limit, namely almost no evolution at all. More precisely, this nucleus is predicted to proceed from small oblate deformations to fission *directly*, i.e., without passing through intermediate equilibrium shapes, in contrast to many other nuclei in which the presence of the high angular momentum induces the superdeformed, intermediate equilibria at high temperatures and/or the Jacobi-type shape transition. We find it instructive to test the actual prediction experimentally.

II. THE EXPERIMENT

The experiment was performed at LNL in Legnaro (Italy) using a 96 MeV ^{18}O beam bombarding a self-supporting target ^{198}Pt (1 mg/cm^2 thick). The bombarding energy was chosen to lead to the angular momentum distribution with $l_{max} \approx 42$, which is slightly larger than the critical spin for fission and therefore allows for a good population of the isomeric states in ^{211}Rn ($T_{1/2}=201$ ns, $I=63/2^-$) and ^{212}Rn ($T_{1/2}=154$ ns, $I=30^+$) through the intense channels $5n$ and $4n$. The corresponding excitation energy of the compound ^{216}Rn nucleus is $E^*=56$ MeV. The main residues of the formed compound nucleus are ^{212,211,210}Rn covering 99% of total evaporation residues. The predicted cross sections for the population of the ^{212,211,210}Rn residual nuclei are shown as functions of spin in Fig. 1. In the left panels, the total fusion-evaporation cross section for ^{212,211,210}Rn is displayed while in the right panels the fraction (in percent) of the population of each residual nucleus is given. All the calculated results were obtained using the statistical model and the Monte Carlo technique. The curves in the top panels correspond to no condition on the high-energy gamma rays required. In contrast, the curves displayed in the bottom panels are obtained with the additional condition of having in the decay leading to the residual nuclei a high-energy gamma ray with $E_\gamma > 8$ MeV. One can see that requiring the presence of a high-energy gamma ray in the GDR region (as it is done in the experiment) implies the selection of events corresponding mostly to the ^{212}Rn residual nucleus. It is characterized by high spins (experimentally selected by the isomer decay). Therefore, on the basis of these results and for the chosen experimental conditions, we do not expect any sizable background due to fission events.

In the experiment, the HECTOR array [9] was employed. High-energy γ rays were measured in eight large BaF_2 detectors, while the prompt, low-energy transitions were detected in 38 small BaF_2 detectors arranged in honeycomb mode above and below the target location and provided the sum energy and the γ ray fold. In addition, a Mylar foil (8 μm) with a central hole (6 mm) placed downstream at 40 cm from the target was employed as a catcher to stop the recoiling residual nuclei. The direct beam and most of the scattered beam passed trough the central hole in the catcher. Because of this hole, the stopping efficiency was only about 28%. The chosen distance $\sim$40 cm was appropriate for the lifetime of the isomeric states of interest, namely 201 ns and 154 ns. The delayed gamma radiation of the stopped residues (deexciting the isomeric states) was measured in a BGO detector. This BGO detector was the standard Compton shield usually used for Ge detectors. Because of its geometry, the BGO shield surrounded the beam line around the catcher, covering a large fraction of the solid angle. In addition, a Ge detector with its BGO shield was placed near the reaction chamber at 146° to measure discrete transitions at the target position. In order to detect the delayed gamma transitions, the beam was pulsed with 10 ns pulses separated by 400 ns intervals.

The trigger condition was the logical sum of the following events: (i) the coincidence of the high-energy γ rays with the multiplicity filter; (ii) the coincidence of the high-energy γ rays with the multiplicity filter and the BGO detector; (iii) single Ge detector firing; (iv) the coincidence of the Ge detector with the BGO detector.

III. EXPERIMENTAL RESULTS

In this section we are going to present various aspects of the experimental analysis and the obtained results, including the analysis of the time spectra, of the fold distributions as well as the statistical model analysis, and the corresponding parametrizations of the GDR curves.

A. Time spectra

In Fig. 2 (top panel), the time spectrum of the gamma radiation emitted by nuclei stopped in the catcher—with respect to a prompt radiation detected with the multiplicity filter around the target—is shown. This spectrum has a rather complicated structure, which results from many different components of various decays involved. In particular, we identify in the spectrum the prompt γ rays from the target, the γ rays produced by the scattered beam in the catcher, and the γ rays emitted by the nuclei with the mass similar to the target mass stopped in the catcher. The events of interest are

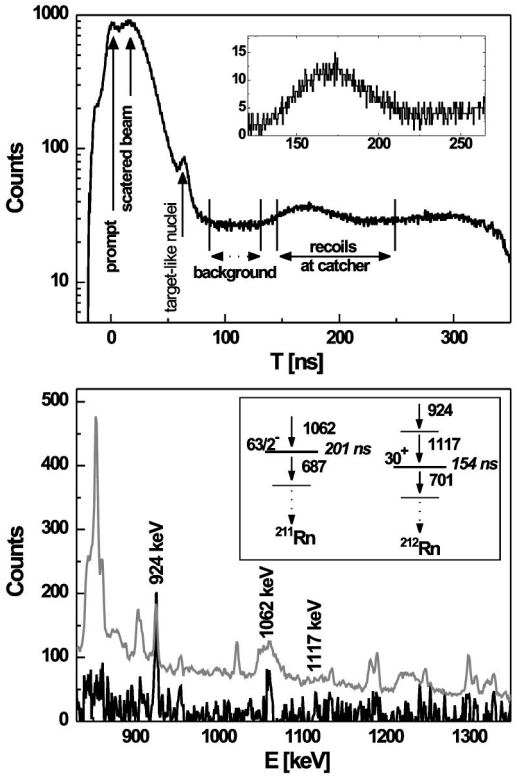

FIG. 2. Top panel: Time-of-flight spectrum measured by the catcher detector around the catcher foil. Regions corresponding to various processes taking place during the measurement are indicated. The region corresponding to the emission from recoils at the catcher is shown in detail in the inset; this spectrum is background subtracted. It corresponds to detection of the γ rays from the isomeric states in ^{211}Rn and ^{212}Rn. Bottom panel: The γ-ray spectrum measured with the Ge detector as obtained without any gate on the time spectrum (gray histogram) compared to the spectrum gated with the isomer part of time of flight (black histogram). The gated spectrum shows an enhancement of the transitions above the isomeric states. The inset to this panel shows the parts of the level schemes of ^{211}Rn and ^{212}Rn with transitions above the isomeric states.

in the region indicated by the horizontal full arrow, which corresponds to the time of flight of fusion-evaporation recoils ($\sim$150 ns) convoluted with the isomeric-decay time distribution. One can see an excess of counts in this region as compared to the overall background. This can be seen more clearly in the inset in Fig. 2, where the region of interest, after background subtraction, is shown in linear scale. In order to investigate the quality of the isomeric-decay selection by using the time gating, in the bottom part of Fig. 2 we compare two Ge spectra: the one without any conditions and the other one, gated by the delayed γ rays (background subtracted) measured by the BGO around the catcher, with the time condition as indicated in Fig. 2 (top). The spectrum gated by the delayed radiation shows mainly the lines corresponding to the prompt transitions feeding the isomeric states (see the inset to Fig. 2, bottom panel). This demonstrates the sensitivity of our gating condition for selecting most of the contributions from the decay chains populating the high-spin isomers. It should also be noted that the observed intensity ratio of 924 and 1117 keV transitions suggests that the transition order should be reversed, compared to that given in Ref. [7].

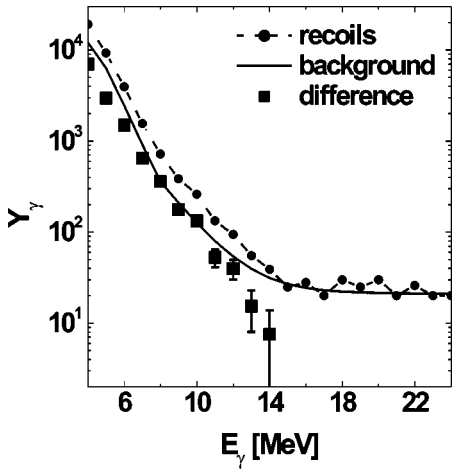

FIG. 3. The spectra of high-energy γ rays for three different conditions: recoils and background corresponding to the gates shown in Fig. 2 and the difference of these two spectra shown with filled squares.

Figure 3 shows the high-energy spectra obtained by gating on "recoils at catcher" and on "background" regions (these regions are shown in the top panel of Fig. 2). The total spectrum denoted as "recoils" contains background in addition to the data corresponding to the isomeric states. The background was eliminated by subtracting the background spectrum from the total one after normalization. The difference is the isomer gated high-energy gamma spectrum used for analysis with the statistical model (see Sec. III C).

B. Fold distributions

The experimental fold distributions measured in the present experiment are shown in Fig. 4. Open squares show the total fold distribution, the full triangles show the fold distribution gated by the isomeric decay, while the full circles show the difference between these two spectra. The latter gives the fold distribution of the total prompt decay which is compared to the calculated ones (lines) assuming a particular l_{max} value, ranging from 33 to 45 $\hbar$. The calculations took into account the multiplicity filter efficiency and the scattering probability (using the method described in [9]). We may remark that (a) the value of l_{max} that gives the best reproduction of the experimental data corresponds to 39 $\hbar$, the spin-value very close to the predicted fission limit; and (b) the fold distribution populating the isomeric state agrees well with the assumption of five transitions (on the average) above the isomeric state, as suggested by the good reproduction of the data with the calculated curve. These two remarks provide additional proof of the good time-gating sensitivity to select the cascades leading to the isomers.

High-energy γ-ray spectra were obtained with the conditions set either on the gamma coincidence-fold or on the time spectrum, in order to select the delayed radiation emitted and detected around the catcher foil. The non-isomer gated spec-

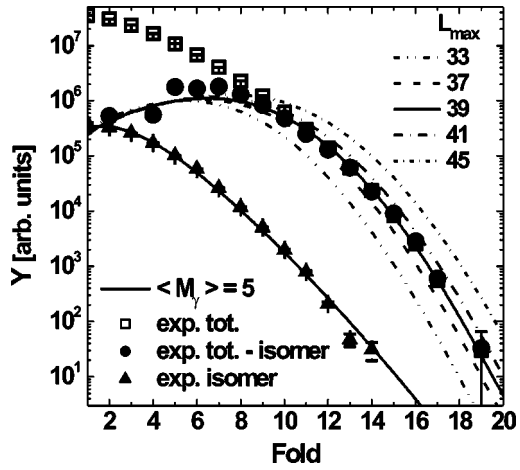

FIG. 4. The experimental coincidence fold-distributions of the low-energy transitions. The data without any conditions on the time-of-flight spectrum of Fig. 2 are marked with the squares, while the triangles correspond to the isomer gated data. The difference of these two distributions (after normalization in the total counts in the fold interval 1–4) is shown with the circles. The lines show the calculated fold distributions, each corresponding to a value of l_{max} in the interval 33 to 45 $\hbar$. The best fit to the data is for $l_{max}=39\ \hbar$ (solid line), while the distribution with the average γ-multiplicity, $M_\gamma=5$, corresponds to the isomer gated data.

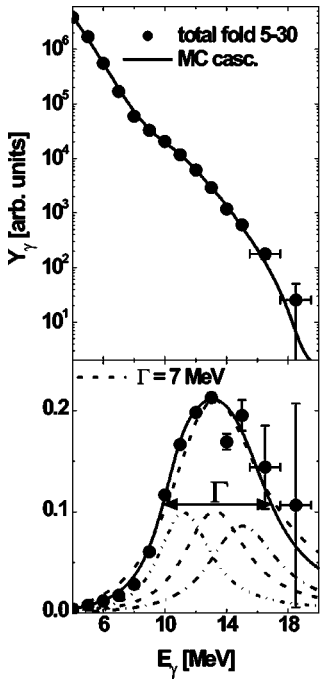

FIG. 5. Top panel: The experimental high-energy γ-ray spectrum corresponding to the folds 5–30 represented with full dots. The line is the result of the best-fit statistical-model calculations. Bottom panel: The data in the linearized form described in the text and the best-fit GDR line shape (solid line) consisting of the sum of three Lorentzian functions. The one-Lorentzian function drawn with the dashed line is compared to the sum (full line) of three Lorentzian components.

tra are taken for folds >4 only, as the lower fold spectra can be contaminated by the reactions other than fusion. The isomer gated high-energy spectrum corresponds to the whole fold region.

C. Statistical model analysis

In this section we present the measured high-energy γ-ray spectra and discuss the comparison with the statistical model predictions which are needed to extract the GDR parameters. All calculations were performed by using the Monte Carlo version of the CASCADE code. In fact, as we will discuss below, only by using the Monte Carlo technique can one obtain predictions corresponding to the evaporation chains leading to the specific residual nuclei.

The first step of the analysis was to obtain the information about the GDR from the high-energy γ-ray spectrum corresponding to the 5–30 range of the γ-fold measured by the multiplicity filter. As discussed in the previous section, in connection with the multiplicity filter data of Fig. 4, this fold interval is expected to select the high energy γ rays mainly coming from fusion-evaporation events. This spectrum, denoted "total", is shown in Fig. 5 and compared to the best-fit statistical-model calculation in which the experimental yrast line and Reisdorf level density model [10,11] were used.

With this Monte Carlo code we produced 1 million events, each consisting of a chain including evaporated-particle type energies and spins as well as the γ-ray properties. This enabled us to sort those events simulating in the best possible way the experimental conditions of selecting the spin of the residual nucleus. The spin distribution of the compound nucleus, given as an input to the code, was deduced from the measured low-energy γ-ray fold-distribution adopting the same procedure described in Ref. [9] which is based on the measured response function of multiplicity filter. To convert the multiplicity to spin, we applied the empirical relation $I=2M-3$ which assumes quadrupole stretched transitions and a correction for the E1 transitions and angular momentum removed by a decay through particle emission. This resulted in $l_{max}=39\ \hbar$, which reproduces very well the measured fold distribution (see Fig. 4).

The GDR parameters (centroid and width) are deduced from the chi-square minimization in the region of γ-ray energy of 8–14 MeV for the isomer gated—and of 8–16 MeV in the total-data—case. We use two approaches for the parametrization of the GDR line shape. The first, similar to that in many previous works, assumes a single Lorentzian function. In this case, the best fit of the GDR width is 7 MeV. The second approach takes into account the fact that the dipole resonance mechanism involves three degrees of freedom usually interpreted in terms of oscillations in three orthogonal directions, and therefore we parametrize its line shape by a superposition of 3-Lorentzians (below abbreviated to 3-L). With this approach, we obtain a better description of the experimental data with an overall GDR width nearly identical to that of the single Lorentzian fit. This is illustrated in the bottom part of Fig. 5, where we compare the data in the linear form and the best-fitted GDR strength function represented by the quantity $F_{3L}(E_\gamma)*Y_\gamma^{exp}(E_\gamma)/Y_\gamma^{cal}(E_\gamma)$. In that expression, $Y_\gamma^{exp}(E_\gamma)$ and $Y_\gamma^{cal}(E_\gamma)$ are the experimental and calculated spectra, respectively. The best-fitting GDR strength

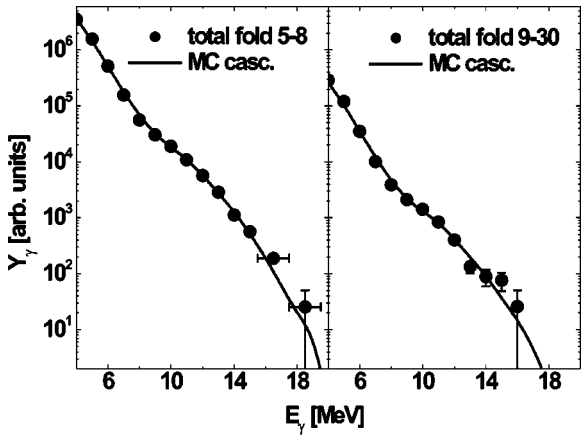

FIG. 6. The experimental spectra (points) corresponding to the selected low-and high-fold regions, and the best-fit Monte Carlo cascade calculations (lines) performed with a value of the GDR width of 7 MeV.

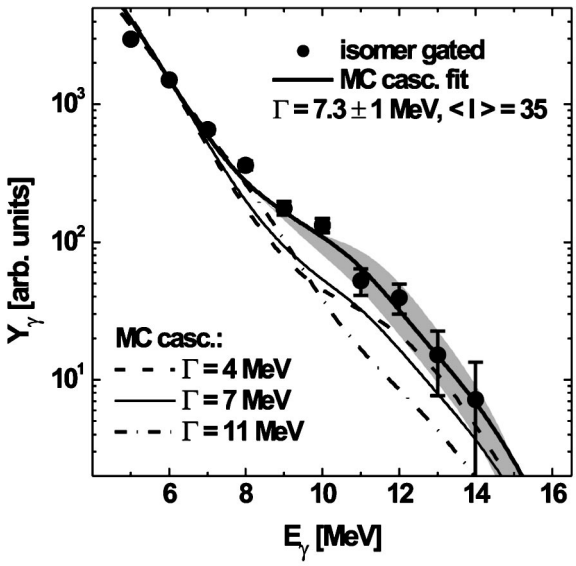

FIG. 7. The experimental high-energy spectrum gated by the isomer decay is shown with the full circles. Four statistical model Monte Carlo calculations are shown with lines. The calculation using the fold interval 5-30 and GDR width of 7 MeV, which corresponds to the best-fit curve of Fig. 5, is displayed as the thin solid line. The calculations corresponding to GDR widths of 4 and 11 MeV are shown with the dashed and dash-dotted lines, respectively. The fit to the isomer gated spectrum obtained for $\Gamma = 7.3 \pm 1$ MeV and assuming only the high-spin region ($\langle I \rangle = 35\ \hbar$) is presented with thick solid line. The shaded area indicates the possible deviations of the calculated GDR spectrum from the best-fit curve within the 1 MeV error bars of the GDR width.

function, $F_{3L}(E_\gamma)$, consists of a three-component Lorentzian function with parameters (energy, width, and strength) taken from the best fit to the experimental spectrum. $F_{3L}(E_\gamma)$ and its individual components are also presented in the figure.

It should be noted that the best-fit $F_{3L}(E_\gamma)$ line is a superposition of three similar Lorentzians positioned at $E_{\mathrm{GDR}} = 11.2$, 13.2, and 15 MeV with the widths of $\Gamma_{\mathrm{GDR}} = 3.5$, 4.5, and 5 MeV, respectively. It has a width of 7 MeV—the result coinciding with the one obtained when using the single-Lorentzian approach. The 3-L approach suggests that the susceptibilities in generating the three orthogonal modes are different, thus implying the observed differences in the Lorentzian factors. Our particular result does not give evidence of the triaxiality; we rather conclude that the shapes involved are not very different from the spherical one, while in terms of the amplitudes of the oscillations related to the three modes some differences do appear.

In the next step of the analysis, we interpret the high-energy γ-ray spectra associated with two different spin regions of the compound nucleus. Figure 6 shows two spectra, the one obtained by gating on the fold 5–8 and the other one by gating on the fold 9–30. They correspond to 10 $\hbar$ wide regions of angular momentum, with the average spin of 23 $\hbar$ and 29 $\hbar$, respectively. The statistical model fits, corresponding to these spin regions, are also displayed in the figure. The 3-L approach, applied here, results in the GDR parameters (centroids and widths) equal to those obtained from total spectrum. The fitted single Lorentzian GDR width is also 7 MeV, in both cases studied.

The most interesting high-energy γ-ray spectrum is the one corresponding to the selection of the delayed low-energy gamma transitions measured around the catcher. In particular, such a spectrum is obtained by gating on the isomer related part of the time spectrum, namely that indicated by the double-end long arrow in Fig. 2, and using as the background the spectrum gated by the part indicated by the dotted arrow. The selection on the population of the isomeric states leads to a high-energy γ-ray spectrum with rather poor statistics, dying out at about the GDR centroid energy.

The isomer gated spectrum is shown in Fig. 7. To see whether or not its shape is very different from that of the total spectrum, the isomer gated data are compared to the best-fit calculation result for the total spectrum (shown with the thin solid line in Fig. 7). There are also shown results of the calculations performed for two other extreme GDR width values, viz., 4 and 11 MeV (dashed and dash-dotted lines, respectively). One can see that none of them can describe the experimental data.

Indeed, the isomer gated spectrum has a shape remarkably different from that of the total spectrum in the whole region of $E_\gamma > 6$ MeV. In this context it is important to stress that the isomer-gated spectrum corresponds to a different spin distribution as compared to the total spectrum and, therefore, it is related to a different region of the phase space of the nuclear decay. Consequently, before trying to fit the spectra by changing the GDR parameters, we have introduced in our simulation the condition of gating on the isomeric decay. This was achieved by performing the Monte Carlo calculations. We used the same parameters as those used in the analysis of the total spectrum. We selected only the cascades leading to the nuclei having the average entry spin of 35 $\hbar$, that is, the average of the angular momentum distribution ranging from 30 $\hbar$ to the l_{max}. This resulted in quite good overall reproduction of the data. Subsequently, in order to fit the isomer-gated spectrum, the calculations for different GDR parameters were made. The best-fit spectrum shown with the thick full line in Fig. 7 was obtained for the GDR width $\Gamma = 7.3 \pm 1$ MeV using χ^2 minimization. It indicates that the GDR width at these very high spins does not differ

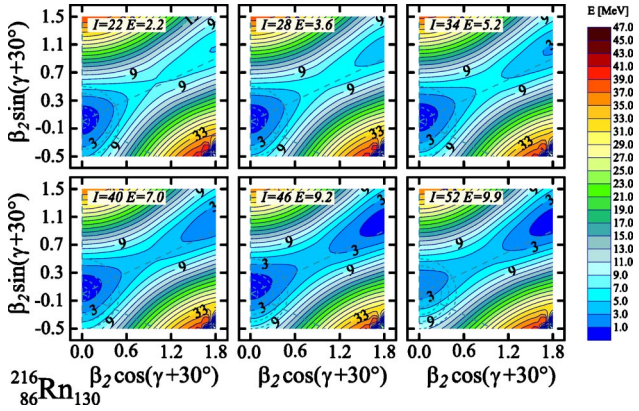

FIG. 8. (Color online) The ^{216}Rn potential energy maps calculated using the LSD model. As one can see, this approach predicts for the ^{216}Rn nucleus an equilibrium shape (*cf. the minima of the potential energy*) which is approximately spherical up to the spins around $I=40\ \hbar$. At $I=40\ \hbar$, the fission barrier is about 3 MeV high, so that for $I \geqslant 40\ \hbar$ the fission decay mode is expected to dominate. Note that the only evolution with spin is the decreasing in the barrier height and no Jacobi transition is expected in this nucleus according to the calculations.

appreciably from the widths obtained at lower spins. In Fig. 7, a shaded area is shown which is limited at the lower and upper extremes by the values corresponding to the GDR width of 8.3 and 6.3 MeV, respectively.

IV. CALCULATION METHOD

It is known from several other studies that the role of the shell effects diminishes with temperature. In doubly magic nuclei, the temperature at which the strong shell effects are smeared out is expected to be of the order of 2 MeV. Outside the doubly closed-shell nuclei, these limiting temperatures are lower and the calculations based on the cranking Strutinsky method (cf., e.g., [12]) indicate that at $T \sim 1$ MeV the corresponding shell effects are usually negligible. Consequently, the results of the macroscopic model calculations for the ^{216}Rn nucleus in the form of the potential energy surfaces shown in Fig. 8 are a realistic approximation of the nuclear energies at the 1 MeV temperature that corresponds to the conditions of the present experiment.

To understand better the shape fluctuation mechanism underlying the experimental conditions of the present study, we would like to obtain the shape distribution with the help of the newest version of the liquid drop model that accounts explicitly for the nuclear-surface curvature effects. These effects are particularly important at large elongations, especially for the neck-forming nuclear configurations, and the corresponding approach is expected to provide a better description, in particular, of the fission barriers. Such a model was recently developed in Strasbourg within the Lublin-Strasbourg collaboration and is further referred to as the Lublin-Strasbourg Drop (LSD) approach [13,14]. It has been shown that the LSD approach provides indeed a more realistic parametrization of the fission barriers as compared to the earlier calculations of this type, and one may expect it to give a more realistic distribution of shapes close to the fission limit. In fact, in the case of the light nucleus ^{46}Ti, the model does predict a Jacobi transition in accordance with the experimental results of Ref. [15].

The technique of calculating the distributions of probability to find a given nucleus at the deformation specified by *an ensemble* of deformation parameters, say $\{\alpha\}$, is fairly standard nowadays (cf. Ref. [16]), and below we give only a few mathematical expressions rendering the presented information reproducible by an independent study.

The probability distribution to find the nucleus at a given deformation is given by the so-called Boltzmann factor, $P = P(\{\alpha\}, I, T)$; in nuclear physics applications it is a function of the ensemble of deformation parameters $\{\alpha\}$, spin I, and the temperature T. To shorten the notation, we omit those three variables and write

$$P \sim e^{-F/kT}, \quad F \equiv E - TS, \tag{1}$$

where F denotes the free energy, E the energy of the system (in the present application set equal to the macroscopic energy obtained from the LSD approach), and S the entropy given by the single-particle level-occupation factors n_ν,

$$S = -\sum_\nu n_\nu \ln n_\nu - \sum_\nu (1 - n_\nu)\ln(1 - n_\nu). \tag{2}$$

The occupation factors depend in fact on the deformation, spin, and temperature as well, but as before, these variables are omitted and we have

$$n_\nu = \frac{1}{1 + \exp[(e_\nu - \lambda)/T]}. \tag{3}$$

The Fermi energy λ is found from the usual particle-number condition

$$(N \text{ or } Z) = \sum_\nu n_\nu. \tag{4}$$

The single-particle energies e_ν are calculated using the deformed Woods-Saxon potential with the universal parameter set (cf. Ref. [17]).

For a given experimental excitation energy E^*, we calculate the thermal excitation energy available to the system, $U = E^* - E$, at each deformation point of the (β, γ) plane of the standard quadrupole deformations. The latter energy can be expressed as the difference of the microscopic thermal energies $\mathcal{E} \equiv \Sigma_\nu n_\nu e_\nu$, viz.,

$$U = \mathcal{E}(\{\alpha\}, I, T) - \mathcal{E}(\{\alpha\}, I, T = 0). \tag{5}$$

Equations (4) and (5) provide the system of nonlinear equations from which T and λ are obtained.

The potential energy surfaces of Fig. 8 were obtained using the LSD approach; they were used to calculate the Boltzmann factors of Eq. (1); the resulting distributions describing the probabilities of finding the nucleus at a given deformation are shown in Fig. 9 of the following section.

The corresponding results were used as input to generate the comparison with the experimental results in terms of the usual observables as discussed in the following section.

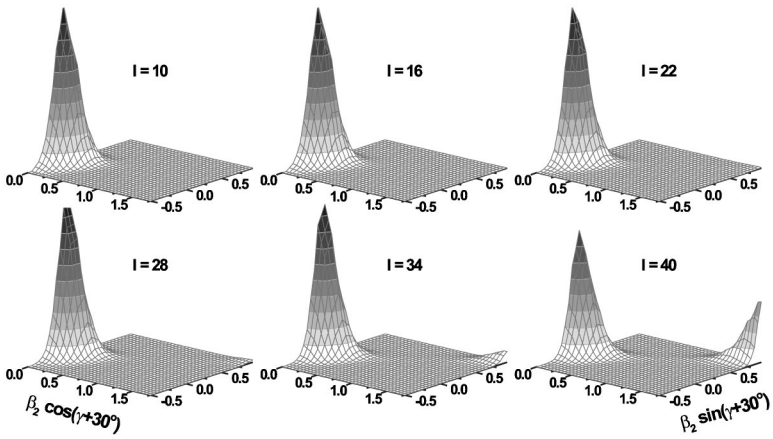

FIG. 9. The probability distributions calculated using the model Boltzmann factors as discussed in the text. Observe the stability of the position of the maximum of the displayed distributions. However, the distributions spread out as a function of spin, their maxima get lower, and, at $I \sim 40\ \hbar$, the traces of the fission path become visible.

V. COMPARISON WITH THEORY AND DISCUSSION

To begin, let us compare the experimental results; all the data for the giant dipole resonance width obtained from the analysis of various spectra are shown in Table I for the hot rotating ^{216}Rn. They correspond to an average temperature of $\langle T \rangle \approx 1$ MeV and to several values of spin which are also reported in the table. It should be noted that the GDR studies performed so far in this heavy mass region were focused on the fission channel. The present study is the first investigation of the GDR width in connection with the fusion-evaporation decay channel.

The measured values of the resonance width are found not to depend strongly on spin, at least in that particular nucleus. They are larger as compared to the zero-temperature widths ($\Gamma_0 \approx 4$ MeV) known from other nuclei in the mass range of interest. This difference is of the same magnitude as that found in lighter nuclei at similar temperature; it has been interpreted in terms of the thermal shape fluctuations. In addition, the fact that the width is not changing in any important way with spin indicates that the effective deformation is not changing significantly with the spin either.

According to the theoretical prediction in Fig. 8, the ^{216}Rn nucleus remains nearly spherical in its ground state; however, the fission barrier decreases from $\sim$9 MeV at $I=10\ \hbar$ to $\sim$3 MeV at $I=40\ \hbar$. Consequently, one should not expect any significant presence of the large deformations in this nucleus at the temperature sufficiently high to wash-out the shell effects. Our experimental results seem to confirm this picture, although *a priori* one cannot exclude the possibility that the sensitivity of this particular experiment is not adequate to sample the presence of very large deformations which could be *weakly populated*.

The width of the Boltzmann distribution reflects the thermal shape fluctuation amplitude, and, therefore, shows the contribution of the shape fluctuations to the overall GDR width. The deformation value corresponding to the maximum of the distribution is the equilibrium deformation. Both the equilibrium deformation and the variance of the distribution play an important role in describing the GDR width. From Fig. 9 one expects that both of these contributions to the GDR width are not changing very much with spin. In fact, only a slight increase of the GDR width can be expected, as the probability distributions become slightly broader, i.e., sampling larger deformation but with very small probability.

The calculation of the GDR line shape obtained within the thermal shape fluctuation model as a sum of all possible line shapes (for all deformation values) weighted with the Boltzmann factor (cf. Ref. [16]) gives the GDR width values plotted as the dashed line in the top panel of Fig. 10. The calculations assume at $T=0$ a spherical shape with a GDR width of 4 MeV. The obtained predictions show that the result of the average over the shape ensemble at $T=1$ leads to an increase of the GDR width which in the present case is about 7 MeV.

In the top panel of Fig. 10, calculation results are compared to the present experimental results and to the predictions based on the same mechanism but using the parametrization reported in [18,19]. Both approaches give the results consistent with the experimental values. In addition, in the bottom part of the figure we display the main features of the calculated liquid drop shape distribution by showing the static equilibrium quadrupole deformation (β_{eq}), average dynamical deformation ($\langle\beta\rangle$), and the standard deviation of the β distribution ($\langle\Delta\beta\rangle$). The static equilibrium deformation is $\sim$0 up to spin 30 $\hbar$, and then slightly increases, while the standard deviation is almost constant with angular momentum. Both static and dynamic deformations determine the shape evolution of the investigated nucleus. It is basically

TABLE I. The GDR parameters for ^{216}Rn obtained from the fit to the experimental data.

Data	Fold 5-8	Fold 5-30	Fold 9-30	Isomer gated
$\langle I \rangle [\hbar]$	23	26	29	35
Γ (MeV)	7.0±0.3	7.0±0.3	7.0±0.4	7.3±1.0
E (MeV)	13.2±0.1	13.2±0.1	13.2±0.3	13.2±0.5

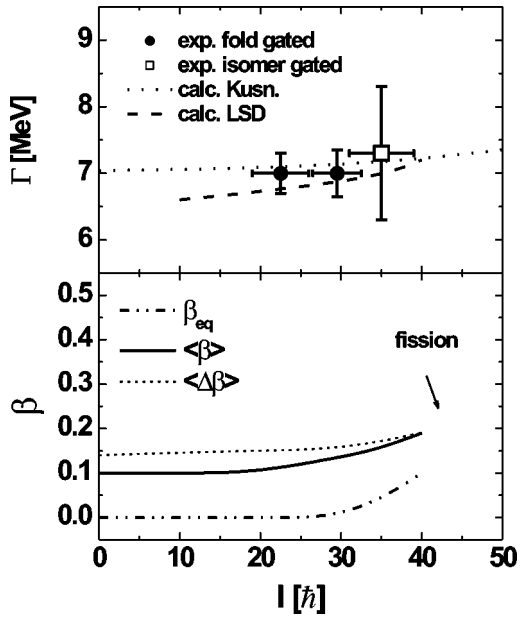

FIG. 10. Top panel: The GDR width as a function of spin obtained for experimental GDR strength functions is shown with points in the top panel in comparison with theoretical predictions (the horizontal error bars correspond to the half-width of the spin distribution selected by the gating conditions). The dotted line corresponds to results of calculations performed according to the Kusnezov formula. The GDR width calculated using thermal shape fluctuations based on potential energies obtained with LSD model is drawn with the dashed line. Bottom panel: The LSD model predictions for equilibrium deformation β_{eq} are presented in the bottom panel with the dash-dotted line. The dashed line $\langle\Delta\beta\rangle$ (square root of the variance of the β distribution) indicates the extent of the possible deformations and $\langle\beta\rangle$ (solid line) is the average deformation.

constant with spin, as is the behavior of the calculated GDR width.

VI. SUMMARY AND CONCLUSIONS

The present work demonstrates the possibility to study the nuclear shape around the fission limit through the GDR γ-decay in exclusive measurements selecting spins and using the isomer tagging technique. The present study is the first investigation of the Giant Dipole Resonance width from the fusion-evaporation decay channel in this nuclear mass range.

Theoretical calculations at zero temperature, Ref. [20], predict a superdeformation in the ^{216}Rn nucleus at the quadrupole deformation $\sim$0.5, with the potential barrier separating the first and the second minima of a moderate size of about 2–3 MeV. At an average temperature of $\langle T\rangle \sim 1$ MeV, the shell effects are about to disappear as discussed in the text. To which extent these two factors, viz., the shell effects and the temperature compete is a crucial question to examine, since the reliable theoretical predictions about the population (or not) of super- and/or hyperdeformed minima must be able to control these two factors reliably. The fact that no sign of the superdeformed (more generally large deformation) shapes has been obtained in the present study can be interpreted as another confirmation of the earlier expectation that *temperatures* $\langle T\rangle \sim 1$ MeV *wash out the potential barriers of at least* $V_b \leqslant 3$ MeV.

According to the present study, the $\langle T\rangle \sim 1$ MeV hot ^{216}Rn nucleus has nearly spherical (static equilibrium) shapes up to spin $I=30$ and weakly oblate deformations when approaching the fission limit at $I=40$. The standard deviation of the thermal shape fluctuation ensemble $\langle\Delta\beta\rangle$ obtained from our calculations is nearly constant in spin. The average dynamical deformation obtained with the Boltzmann factor described in the text is rather small ($\sim$0.15) and does not change either with angular momentum within the studied range.

The fact that the ^{216}Rn nucleus investigated here was found to be almost spherical up to the fission limit is perhaps not surprising given the fact that the results of the calculations were known prior to the experiment; however, the extent to which this result agrees with the calculations suggests that the progress achieved within the LSD approach is indeed encouraging. This has further implications: since the LSD-model parameters are independent of the nucleus studied here (they were fitted to all the experimental masses known contemporarily), the parameter-free description of the Jacobi transition in ^{46}Ti of Ref. [15] and simultaneously of the no-Jacobi transition in ^{216}Rn of this study provides important test cases. However, obviously more such test cases in various mass ranges will be needed to claim the full success of the new description of the nuclear macroscopic energies.

ACKNOWLEDGMENTS

This work was supported by the Polish State Committee for Scientific Research (KBN Grant No. 2 P03B 118 22), the Italian INFN, LNL Legnaro, and the Danish Sciences Foundation. A contribution from the exchange program between the *Institut National de Physique Nucléaire et de Physique des Particules*, IN_2P_3, and Polish Nuclear Physics Laboratories is acknowledged.

[1] K. A. Snover, Annu. Rev. Nucl. Part. Sci. **36**, 545 (1986).
[2] J. J. Gaardhøje, Annu. Rev. Nucl. Part. Sci. **42**, 483 (1992).
[3] P. Bortignon, A. Bracco, and R. A. Broglia, *Giant Resonances: Nuclear Structure at Finite Temperature* (Gordon & Breach, New York, 1998).
[4] R. Butsch *et al.*, Phys. Rev. C **41**, 1530 (1990).
[5] T. Tveter *et al.*, Phys. Rev. Lett. **76**, 1035 (1996).
[6] F. Camera *et al.*, Phys. Rev. C **60**, 014306 (1999).
[7] G. D. Dracoulis *et al.*, Phys. Lett. B **246**, 31 (1990).
[8] J. P. S. van Schagen *et al.*, Nucl. Phys. **A581**, 145 (1995).

[9] A. Maj *et al.*, Nucl. Phys. **A571**, 185 (1994).
[10] M. Kicińska-Habior *et al.*, Phys. Rev. C **41**, 2075 (1990).
[11] W. Reisdorf, Z. Phys. A **300**, 227 (1981).
[12] J. Dudek, B. Herskind, W. Nazarewicz, Z. Szymański, and T. R. Werner; Phys. Rev. C **38**, 940 (1988)
[13] K. Pomorski and J. Dudek, Phys. Rev. C **67**, 044316 (2003).
[14] J. Dudek and K. Pomorski, Eur. Phys. J. A (to be published), nucl-th/0205011.
[15] A. Maj *et al.*, Nucl. Phys. **A731**, 319 (2004).
[16] W. E. Ormand, P. F. Bortignon, and R. A. Broglia, Nucl. Phys. **A618**, 20 (1997).
[17] S. Ćwiok, J. Dudek, W. Nazarewicz, J. Skalski, and T. R. Werner, Comput. Phys. Commun. **46**, 379 (1987), and references therein.
[18] D. Kusnezov, Y. Alhassid, and K. A. Snover, Phys. Rev. Lett. **81**, 542 (1998).
[19] D. Kusnezov and W. E. Ormand, Phys. Rev. Lett. **90**, 042501 (2003).
[20] T. R. Werner and J. Dudek, At. Data Nucl. Data Tables **59**, 145 (1995).